Geochemistry Geophysics Geosystems G3

Published by AGU and the Geochemical Society

Article
Volume 13, Number 1
1 February 2012
Q0AK03, doi:10.1029/2011GC003873
ISSN: 1525-2027

The importance of slab pull and a global asthenosphere to plate motions

Joost van Summeren and Clinton P. Conrad
Department of Geology and Geophysics, University of Hawai'i at Mānoa, 1680 East-West Road, Honolulu, Hawaii 96822, USA (summeren@hawaii.edu)

Carolina Lithgow-Bertelloni
Department of Earth Sciences, University College London, Gower Street, London WC1E 6BT, UK

[1] Earth's subducting plates move 3–4 times faster than its overriding plates, but it remains unclear whether these contrasting plate speeds are caused by additional pull from subducting slabs or by increased viscous drag on the lithosphere-asthenosphere boundary beneath deeply-protruding continental roots. To investigate the relative importance of plausible controls, we predicted global patterns of plate motions using numerical models that incorporate the influence of subducting slabs, convective mantle flow, and continental roots. From the mantle convection models, we computed a set of dynamically consistent plate velocities by balancing forces that drive and resist the motion of each plate. When deep continental roots anchor to the sub-asthenospheric upper mantle, the calculated patterns of plate motions are close to the observations if only ~20% of (excess) upper mantle slab weight contributes to the slab pull force. However, this small contribution causes plates to move too slowly on average unless mantle viscosity is a factor of ~2 lower than expected from post-glacial rebound. In contrast, we show that predicted and observed plate motions are more easily reconciled if even the deepest continental roots are underlain by a low-viscosity layer and at least half of (excess) upper mantle slab weight contributes to the slab pull force. This preferred scenario agrees with recent seismological evidence for a global asthenosphere and previously proposed mechanisms for partial decoupling of slabs from surface plates.

Components: 8500 words, 5 figures.

Keywords: asthenosphere; continental roots; lithosphere; mantle convection; plate motions; plate-slab coupling.

Index Terms: 8103 Tectonophysics: Continental cratons; 8155 Tectonophysics: Plate motions: general (3040); 8159 Tectonophysics: Rheology: crust and lithosphere (8031).

Received 13 September 2011; **Revised** 22 December 2011; **Accepted** 22 December 2011; **Published** 1 February 2012.

van Summeren, J., C. P. Conrad, and C. Lithgow-Bertelloni (2012), The importance of slab pull and a global asthenosphere to plate motions, *Geochem. Geophys. Geosyst.*, *13*, Q0AK03, doi:10.1029/2011GC003873.

Theme: The Lithosphere-Asthenosphere Boundary

Copyright 2012 by the American Geophysical Union

1. Introduction

[2] The observation that subducting plates move three to four times faster across Earth's surface than overriding plates [*Forsyth and Uyeda*, 1975] has been long-recognized as providing a constraint on plate-tectonic forces and upper mantle structure. Although the directions of observed plate motions are consistent with plate forces associated with convective flow in Earth's mantle [*Lithgow-Bertelloni and Richards*, 1998], the relative rapidity of oceanic plates requires an additional mechanism. One plausible mechanism is the pull of slab weight on subducting plates via guiding stresses transmitted within the slab [*Elsasser*, 1969]. Stresses are transmitted more efficiently within stronger slabs and, hence, slab rheology exerts an important influence on the slab pull force. By imposing the weight of slabs as a one-sided edge force to plate boundaries, *Conrad and Lithgow-Bertelloni* [2002] demonstrated that predicted motions of uniform thickness plates agree best with observed motions when slab pull and mantle flow contribute approximately equally to plate driving forces.

[3] Plate motions may also be modulated by lithospheric structure. A variety of geophysical evidence [*Jordan*, 1975; *Rudnick et al.*, 1998; *Hirth et al.*, 2000] suggests that continental roots below old cratons protrude hundreds of km into the mantle. The influence of these roots on plate motions depends on their thickness, geometry, and rheology, and additional coupling between continental plates and mantle flow may enhance either plate-driving basal tractions [*Alvarez*, 1982] or the viscous mantle drag that acts to resist plate motion [*Forsyth and Uyeda*, 1975; *Carlson*, 1981]. Numerical modeling has demonstrated that cratons generally reduce continental plate speeds, particularly if roots protrude below the low-viscosity asthenosphere and couple mechanically to the deeper, more viscous part of the mantle [*Zhong*, 2001; *Becker*, 2006].

[4] Despite the potential importance of both slab pull and continental roots, their relative influence on global patterns of plate motions has not yet been determined. To help disentangle the various controls of Earth's plate motions, we constructed numerical models that combine (1) lateral viscosity variations associated with continental roots, (2) a global parameterization of slab pull edge forces, and (3) plate-driving forces associated with convective mantle flow inferred from seismic tomography images of mantle structure. Unlike previous numerical work in which plate motions are prescribed a-priori, we computed sets of plate motions that are consistent with given combinations of slab pull and basal tractions on plates. For this purpose, we used the torque balance method of *Ricard and Vigny* [1989] and *Lithgow-Bertelloni and Richards* [1998] that we have adapted to incorporate both slab pull forces and enhanced plate-mantle coupling beneath cratons. By comparing predicted and observed patterns of plate motions, we place constraints on the rheology of the upper mantle, which modulates plate-mantle coupling at the lithosphere-asthenosphere boundary.

2. Methods

2.1. Torque Balance Method

[5] We predicted a self-consistent set of plate motions, using the torque balance method [*Ricard and Vigny*, 1989]. Mechanical equilibrium of tectonic plates requires a zero net torque on each plate [*Solomon and Sleep*, 1974]. Within this no-net torque requirement, and for a linearized system of equations, we can solve for the motions of tectonic plates by dividing the problem into two parts. First, a "driving torques" vector, $\vec{Q}$, contains the forces associated with slab pull and basal tractions from mantle flow exerted on plates subject to a no-slip surface boundary condition (see section 2.3). Vector $\vec{Q}$ consists of $3N$ elements with 3 vector components for each of N tectonic plates. Second, matrix $\mathbf{M}$ (dimension $3N \times 3N$), represents the resistive forces in the system and contains information about plate geometry and viscosity structure. Diagonal elements of $\mathbf{M}$ represent viscous drag forces exerted on a plate by the mantle over which that plate moves. Off-diagonal elements represent the influence that a plate's motion exerts on other plates via induced mantle flow. We construct matrix $\mathbf{M}$ by prescribing the plate geometry and rotating each plate about a pole of rotation with unit cartesian coordinates (see section 2.2). Torque balance implies that, for every individual plate and for all plates, the driving torques, $\vec{Q}$, must balance the resistive torques, which are given by the product of $\mathbf{M}$ and the vector $\vec{\omega}$ that contains 3 components of the Euler rotation vector for each of N tectonic plates. Thus,

$$\vec{Q} = \mathbf{M}\vec{\omega}. \quad (1)$$

[6] To predict a set of plate motions that is consistent with the driving forces, we invert the above matrix-vector system to solve for rotation vector ω, using singular value decomposition. Within the torque balance method, plate motions are constrained up

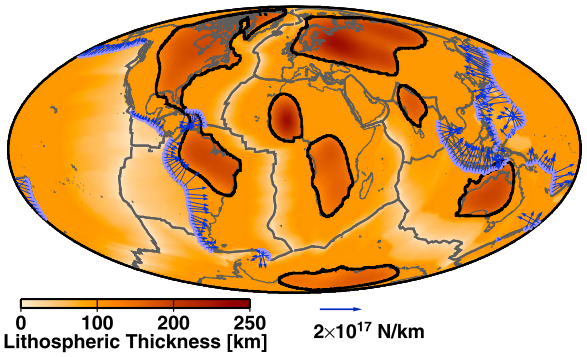

Figure 1. Lithospheric thickness models and slab pull plate-driving forces. Blue arrows depict slab pull edge forces for individual subduction segments. Background colors show lithospheric thicknesses for a model with shallow continental roots (i.e. our second model type, with an asthenospheric channel beneath cratonic roots, section 2.4). Black contour lines surround regions where, for our model with deep continental roots (i.e. our third model type, section 2.4), thick lithosphere reaches the base of the asthenosphere at 300 km and couples mechanically to the underlying, more viscous upper mantle.

to an arbitrary net rotation of the lithosphere with respect to a stable lower mantle [*Ricard and Vigny*, 1989]. Because it is not possible to compute a unique net rotation from our models, we computed the unique set of relative plate motions and express them in a no-net rotation reference frame, for comparison to the (no-net rotation) plate motion model NNR-NUVEL-1A [*DeMets et al.*, 1994]. Furthermore, any possible comparison to absolute plate motions is hampered by uncertainty of the west-trending lithospheric rotation magnitude, where estimates vary from ~1 to ~5 cm yr^{-1} between different models [*Le Pichon*, 1968; *Morgan*, 1971; *Burke and Wilson*, 1972; *Minster et al.*, 1974; *DeMets et al.*, 1990; *Gripp and Gordon*, 2002]

2.2. Plate-Resistive Forces

[7] Resistive torques are computed by prescribing the plate geometry and rotating each plate about a rotation vector with unit cartesian coordinate. The imposed plate velocity is resisted by viscous mantle drag and induces a mantle flow that drives the other plates. To determine individual contributions to the resisting torques, we integrate the basal shear stresses, τ_j, associated with unit rotation of a single plate in one direction (component j), over the lithospheric base of plate P about another direction (component i) [*Lithgow-Bertelloni and Richards*, 1998]:

$$q_{ij} = \int_{A_P} \vec{r} \times \vec{\tau}_j \, dA. \qquad (2)$$

[8] The components of matrix **M** in equation (1) are then given by $M_{ij} = q_{ij}/\omega_j$. The lithospheric base is defined by a viscosity contour that depends on the specific model, as described in section 2.4.

[9] To minimize the artifact of large stresses near plate boundaries due to discontinuous plate velocities, we assign low-viscosity (one tenth times the reference viscosity) to imposed weak zones within 300 km of plate boundaries. Our weak zone parameterization was chosen as the best compromise between tolerable stress buildup near plate boundaries, numerical stability, and a weak sensitivity of the plate motion patterns (see section 2.5) to weak zone parameterization. We found that for an increase of the weak zone viscosity by a factor of 10, the misfit function and plate speed ratio (see section 2.5) change by only 10% and 15%, respectively. Changing the weak zone width to 200 km or 400 km has a similarly small influence on the results.

2.3. Plate-Driving Forces

2.3.1. Slab Pull

[10] Contributions to plate-driving forces from slab pull (Figure 1, blue arrows) are determined from a global compilation of 202 subduction zones [*Wu et al.*, 2008]. For each subduction segment, a one-sided slab pull boundary force couples directly to subducting plates and is estimated from (1) the slab thickness that depends on the plate age at the time of subduction, (2) the excess density of the slab, based on an initial 1200 K temperature difference across the subducting plate, and (3) the vertical extent of slabs in the upper mantle ($z < 670$ km), determined from regional seismic tomography studies [*Lallemand et al.*, 2005]. Slabs contribute to lower mantle downwellings in our models, but we excluded the direct pull of slab material deeper than 670 km because lower mantle slabs are likely dynamically supported in a lower mantle that is 1–2 orders of magnitude more viscous than the upper mantle, consistent with a variety of geophysical data [*Hager*, 1984; *Lambeck and Johnston*, 1998; *van der Hilst et al.*, 1991; *Tao and O'Connell*, 1993]. Although we include slab pull in our torque balance, recent high-resolution modeling allows for more detailed slab geometries and study of back-arc extension and slab rollback [*Stadler et al.*, 2010]. Study of such regional dynamics is beyond the scope of this paper.

[11] To account for uncertainty in the ability of slabs to transmit their entire excess (upper mantle) weight to the surface plates, we apply a global

multiplication factor to the parameterized slab pull forces. We vary this "slab pull fraction" between f_{sp} = 0% (no slab pull) and f_{sp} = 100% (pull due to the slab's entire excess upper mantle weight). We compute the associated slab pull torques using the pull forces shown in Figure 1 (blue arrows). Several mechanisms can reduce the effective slab pull that may evolve during progressive stages of subduction. For example, if the slab is not strong enough to transmit the entire pull force, slabs may become decoupled at shallow depths via stretching, tearing, or detachment [*Spakman et al.*, 1988; *Davies and von Blankenburg*, 1995; *Gerya et al.*, 2004; *Bilek et al.*, 2005]. In addition, part of the slab's potential energy may dissipate due to slab bending [*Chapple and Forsyth*, 1979], although several recent numerical [*Capitanio et al.*, 2007], laboratory [*Schellart*, 2004], and analytical [*Buffett and Heuret*, 2011] studies indicate that lithospheric bending may not be a major energy sink. Resistance to subduction at the fault zone can further reduce the effective slab pull, but depends on the complex interplay between the subducting and overriding plates, and the mantle [*Billen*, 2008; *van Dinther et al.*, 2010]. At depth, upper mantle slabs can be dynamically supported by viscous stresses, which may explain a transition of earthquake focal mechanisms from down-dip extension to compression in the mid-upper mantle [*Isacks and Molnar*, 1971; *Alpert et al.*, 2010]. Locally, magnification of pull forces is possible due to compositional effects, for example, in regions where density increases due to extensive eclogite formation [*Cloos*, 1993; *van Thienen et al.*, 2005]. Because of the uncertain significance of the above mechanisms, we treat the slab pull fraction (f_{sp}) as a free parameter in our models.

2.3.2. Mantle Tractions

[12] In addition to slab pull, mantle convective flow contributes to the plate-driving forces. We compute this driving torque for each plate by integrating the tractions associated with mantle flow over the lithospheric base of each plate. The total driving torque ($\vec{Q}$ in equation (1)) is the vector sum of the torques from slab pull and mantle tractions.

[13] Viscous mantle flow is driven by density heterogeneity derived from the global seismic tomography model S20RTSb [*Ritsema et al.*, 2004]. To convert shear wave velocity anomalies into density anomalies, we employed a uniform tomography conversion factor $\partial\rho/\partial v_S$ = 0.15 g cm^{-3} km^{-1} s, consistent with estimates from mineral physics [*Karato and Karki*, 2001] and used in previous studies [e.g., *Steiner and Conrad*, 2007]. We quantified the influence of $\partial\rho/\partial v_S$ for our results in section 4. We excluded buoyancy variations above 300 km because seismic anomalies of compositional origin are likely prominent in this region [*Jordan*, 1975], although we do account for rheological heterogeneity in this region to investigate the influence of continental roots (see section 2.4). This choice, while simplifying our models in continental regions, potentially excludes important heterogeneity beneath oceanic regions. Convection-related stresses vary relatively little between different tomography models [*Becker and O'Connell*, 2001]. We did not consider mantle buoyancy of compositional origin that is likely in the deep lower mantle [*Kellogg et al.*, 1999; *van Summeren*, 2008], although doing so may help improve the fit to plate motions in some areas [*Forte et al.*, 2009]. It is important to note that slabs that reach deeper than 300 km contribute to both slab pull and slab suction in our models (if f_{sp} > 300/670 = 0.45). Although the resolving power of S20RTSb is improved due to the inclusion of surface wave overtones [*Ritsema et al.*, 2004], short wavelength slab signatures are likely underresolved, and this reduces the influence of double counting between 300 and 670 km. Indeed, excluding upper mantle buoyancy entirely, to avoid double counting, has a minor effect on our results (section 4).

[14] We computed instantaneous convective flow of an incompressible Newtonian fluid by solving conservation equations for mass, momentum, and energy using the Boussinesq formulation. The coupled set of convection equations must be solved using the finite element method, instead of within the spectral domain, to better account for lateral viscosity heterogeneity. We use the CitComS-3.1.1 finite element package [*Zhong et al.*, 2000] to calculate flow in 3-dimensional spherical geometry. To yield a stable numerical solution, we use a finite element resolution of 0.86° (or 96 km at the surface) in the lateral direction and we assign 57 nodes in the radial direction with grid refinement to 17 km towards the surface boundary.

2.4. Lithospheric and Asthenospheric Rheology

[15] The key innovation of this study involves predicting the motions of 13 tectonic plates self-consistently in the presence of strong lateral viscosity heterogeneity that results from continental roots. This distinguishes our work from studies with laterally homogeneous rheology [*Lithgow-Bertelloni and Richards*, 1998; *Conrad and Lithgow-Bertelloni*,

2002]. To account for upper mantle rheological heterogeneity, we employed temperature-dependent viscosities in the top 300 km of the mantle domain, following the method of *Behn et al.* [2004]. We imposed an error-function temperature profile with characteristic lithospheric thicknesses and assigned temperature-dependent Arrhenius-type viscosity to the temperatures, following *Conrad and Gurnis* [2003]. To achieve surface plate rigidity, we assign maximum lithospheric viscosities of 10 times the upper mantle viscosity, which we use as the reference value. Our choice of lithospheric viscosity is consistent with studies that compare modeling results to observed plate motions and the geoid [*Ricard et al.*, 1989, 1993; *Lithgow-Bertelloni and Richards*, 1998; *Becker*, 2006; *Ghosh et al.*, 2010]. The viscosity decreases asymptotically to the asthenospheric viscosity, which is taken as 100 times lower than the lithospheric viscosity. Below 300 km, we assign the reference viscosity to an upper mantle layer (300–670 km) and a viscosity 50 times larger for the lower mantle (670–2870 km). The predicted global average plate speed varies inversely with the absolute reference viscosity, which is treated as a free parameter in our models and adjusted to match the absolute average NNR-NUVEL-1A plate speed.

[16] We employed three types of models with contrasting lithospheric rheology. In a first set of models, we assigned uniform lithospheric thicknesses of 100 km (or, lithospheric age of 80 Myr). These models lack lateral viscosity variations, except for plate boundary weak zones (section 2.2), and are thus similar to previous models that employ layered viscosity structures [*Lithgow-Bertelloni and Richards*, 1998; *Becker and O'Connell*, 2001; *Conrad and Lithgow-Bertelloni*, 2002]. However, for consistency with our other model types, we impose a uniform viscosity decrease with depth within the lithospheric layer.

[17] A second set of models features "shallow" continental roots, where plate thickness is not uniform but is instead based on lithospheric ages and seismological data (Figure 1). The characteristic lithospheric thickness varies with the square-root of lithospheric age in oceanic settings [*Müller et al.*, 1997]. For continental settings, lithospheric thicknesses are defined as the maximum depth for which seismic SV-wave velocity anomalies are consistently greater than +1.5% in the global seismic tomography model SAW16AN [*Gung et al.*, 2003]. This model accounts for seismic anisotropy to avoid misinterpretation of flow-related anisotropic fabric as seismically fast continental roots. To maintain continuity at ocean-continent boundaries, we impose maximum and minimum thicknesses of 100 km for oceanic and continental settings, respectively. In these models, all continental roots are underlain by low-viscosity asthenospheric material, which extends between the lithospheric base and 300 km depth.

[18] A third model set has "deep" continental roots (Figure 1, thick dashed contours) that extend to the base of the asthenosphere, which is at a constant depth of 300 km in our models. These models are similar to shallow roots models, except that the part of the lithosphere in excess of z = 100 km was thickened such that the edges of cratons are steepened and the low-viscosity channel is eliminated beneath cratons, i.e. for the regions enclosed by the black contours in Figure 1. In these regions, deep roots protrude into the more viscous sub-asthenospheric upper mantle (Figure 1, black contours).

[19] To investigate the influence of mechanical decoupling of an asthenospheric layer of low viscosity, we tested cases with and without an asthenosphere for the above three model types. For cases with an asthenosphere, the viscosity decreases with depth from the surface to one tenth of the reference (upper mantle) viscosity. For "no-asthenosphere" cases, the asthenospheric viscosity is equal to the reference viscosity. The base of the lithosphere is defined by a viscosity contour that corresponds to similar contour depths for cases with and without an asthenosphere of 0.5 and 2.4 and times the reference viscosity, respectively.

2.5. Plate Motion Diagnostics

[20] We compared model predictions of plate motions to observations, using 3 diagnostics. First, the misfit function [*Conrad and Lithgow-Bertelloni*, 2002] is the average magnitude of vector differences between predicted and observed plate motions, where predicted plate speeds are first normalized so that their average speed matches that of observed plate motions. Thus, a perfect fit (zero misfit) would require matching both azimuths and relative magnitudes of predicted and observed plate velocities at all locations. Second, the ratio of (area-weighted) subducting to overriding plate speeds is compared to the observed value for Earth of ~3.5 [*DeMets et al.*, 1994]. Because predicted plate motions are relative (instead of absolute), they can be compared directly with the NNR-NUVEL-1A plate motions within a no-net rotation reference frame. All major continents are on overriding plates, except Australia, which is counted as a subducting plate. Third, we calculated the sub-lithospheric upper mantle (z < 670 km) viscosity for which predicted global average

plate speed magnitudes (that vary inversely with the absolute mantle viscosity) match the NNR-NUVEL-1A average value of 3.7 cm yr^{-1}. We average the viscosity by using strain-rate weighting, $\eta_{aver} = e^2_{asth}\eta_{asth}d_{asth} + e^2_{um}\eta_{um}d_{um}$, as proposed by *Parmentier et al.* [1976], with viscosity η, strain-rate e, and layer thickness d. The subscripts "asth" and "um" refer to the asthenosphere (100–300 km) and sub-asthenospheric upper mantle (300–670 km), respectively. We assume continuity of stresses at the interface ($e_{asth}\eta_{asth} = e_{um}\eta_{um}$) and obtain the following expression for average upper mantle viscosity:

$$\eta_{aver} = \frac{d_{asth}/\eta_{asth} + d_{um}/\eta_{um}}{d_{asth}/\eta^2_{asth} + d_{um}/\eta^2_{um}} \quad (3)$$

[21] We compare this predicted viscosity to constraints on the viscosity of the sub-lithospheric upper mantle of $\eta = 3–6 \times 10^{20}$ Pa s, obtained from post-glacial rebound analysis [*Mitrovica*, 1996]. Slight differences between upper mantle viscosity estimates [e.g., *Kaufmann and Lambeck*, 2000] make this diagnostic less powerful than our misfit and plate speed ratio diagnostics.

3. Results

[22] We evaluate our model results by examining plate driving and resisting tractions (Figure 2), plate motion diagnostics (Figure 3), and patterns of predicted plate velocities (Figure 4). We use tractions from a model with uniform thickness plates above a low-viscosity asthenosphere (Figures 2a and 2b) to form a reference model to which we compare other models (Figures 2c–2h). Note that, in the comparison of tractions, a small difference in the location of zero crossings can result in locally large magnitudes of the normalized tractions. Such fluctuations are apparent in the Caribbean, near Bolivia, and on the Antarctic plate south of Africa (Figures 2c–2h), but are unimportant to the force balance because of their near-zero absolute values.

3.1. Influence of a Low-Viscosity Asthenospheric Layer

[23] For the no-asthenosphere cases, mantle flow drives plates in directions that generally agree with the NNR-NUVEL-1A data, but a large contribution of slab pull forces ($f_{sp} \sim 100\%$) is required to bring the plate speed ratio ($V_{subd.}/V_{non-subd.}$) and plate motion directions close to the inferred values for Earth (Figures 3a and 3b (blue curves) and Figures 4a and 4b). The three models without an asthenosphere have almost similar plate motion patterns (Figure 3, blue curves) because the shearing layer over which the plates move (i.e. the entire sublithospheric upper mantle if there is no asthenosphere) is similar for all models. The required slab pull contribution of $f_{sp} \sim 100\%$ is larger than for the reference model with an asthenosphere ($f_{sp} \sim 50–100\%$, Figures 3a and 3b, orange curves) because plate-resisting tractions are larger by a factor of ~4, while plate driving tractions are larger by only a factor of ~2.5 (Figures 2c and 2d). In general, the increase in driving shear tractions is smaller than the increase of resistive tractions because (plate-driving) mantle flow can readjust to reduce strain-rates in regions of strong plate-mantle coupling, but cannot do so if surface plate motions are imposed.

[24] Our results for models without an asthenosphere are consistent with previous results that employ a layered viscosity structure [*Conrad and Lithgow-Bertelloni*, 2002]. Here we demonstrate, however, that the no-asthenosphere models with $f_{sp} = 100\%$ require an upper mantle viscosity that is nearly double the upper bound of the post-glacial rebound estimate by *Mitrovica* [1996] (Figure 3c, blue curves). Accordingly, by using the inferred upper bound for upper mantle viscosity from post-glacial rebound analysis (dark blue star in Figure 3c), the calculated global average plate speed of $V_{aver} = 7.1$ cm yr^{-1} (Figure 4b) is nearly twice the NNR-NUVEL-1A value of 3.7 cm yr^{-1}.

3.2. Shallow Continental Roots

[25] For shallow continental roots over a low-viscosity asthenosphere, plate motions (Figure 4c) are similar to the reference case of uniform plate thickness plates over an asthenosphere, because the low-viscosity asthenosphere permits mechanical plate-mantle decoupling in both models. Relative to the reference model, shear stresses are larger at thick continental roots and lower at thin young oceanic lithosphere, although the differences are modest (mostly between a factor of ~0.5–2, Figures 2e and 2f). In accord with the results of section 3.1, the increase of resisting tractions exceeds the increase of driving tractions. Locally enhanced mantle drag preferentially slows overriding plates and, as a consequence, plate speed ratios increase by ~10% (Figure 3b). However, due to the similarity between uniform models and models with shallow roots, the optimum values for the slab pull contribution are $f_{sp} \gtrsim 50\%$ for both cases (Figures 3a and 3b, red and orange curves). Although the misfit and plate speed

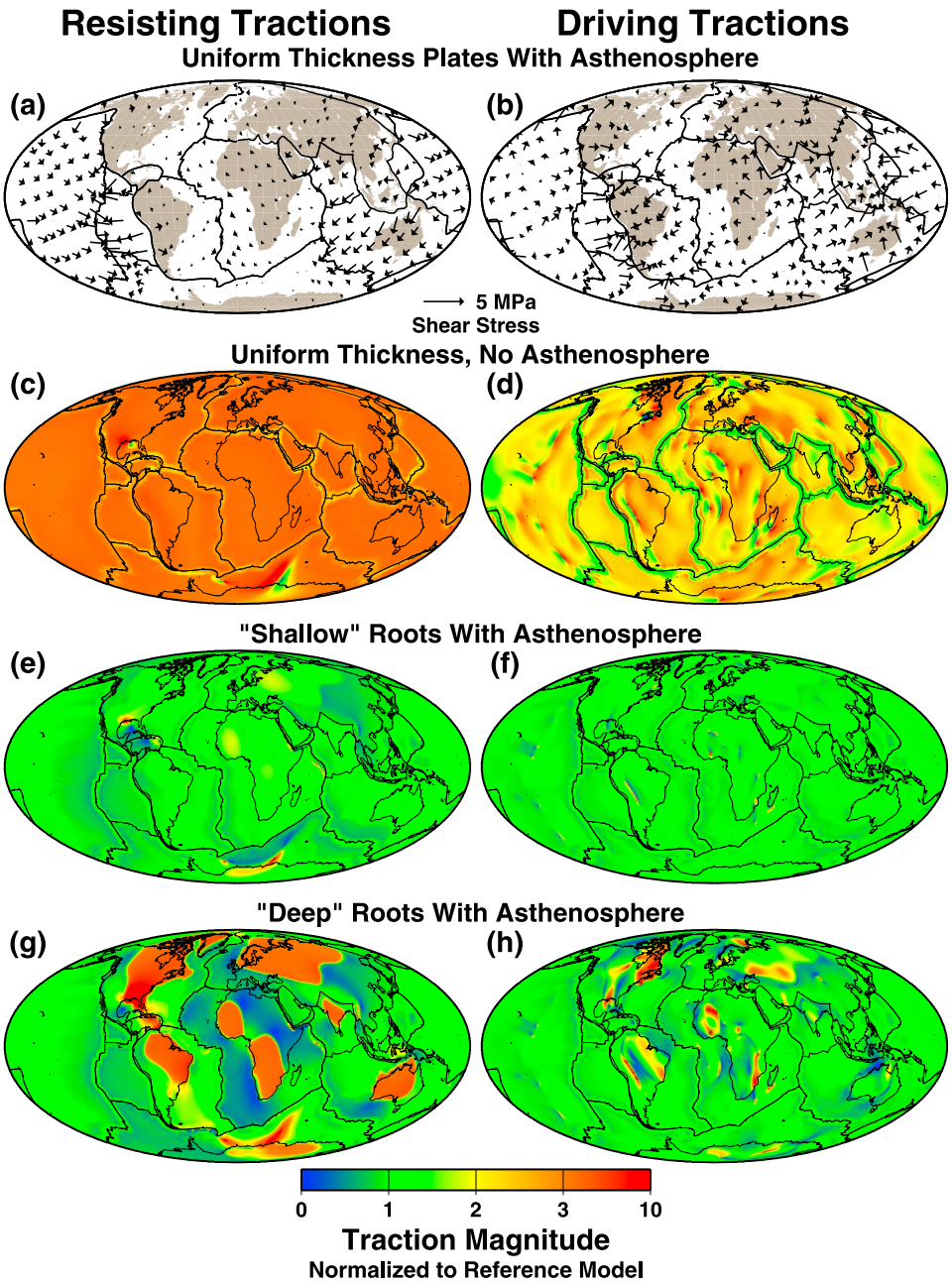

Figure 2. (a) Plate-resisting tractions for a reference model with uniform lithospheric thickness and an asthenosphere. The tractions reflect resistance to NNR-NUVEL-1A plate velocities [*DeMets et al.*, 1994] and are calculated at the base of the lithosphere. (b) Plate-driving tractions associated with mantle convective flow for the same reference model as in Figure 2a. (c–h) Plate-resisting (Figure 2, left) and plate-driving (Figure 2, right) tractions for models of different lithospheric structure compared to the tractions for the reference model shown in Figures 2a and 2b. The three comparison models are described in section 2.4 and are characterized by having no asthenosphere and uniform plate thicknesses (Figures 2c and 2d); shallow continental roots that do not protrude below the low-viscosity asthenosphere (Figures 2e and 2f); and deep continental roots that protrude to the upper mantle below the asthenosphere (Figures 2g and 2h).

ratio diagnostics allow weak slab pull contributions ($f_{sp} \gtrsim 20\%$), the upper mantle viscosity required to match observed speeds requires $f_{sp} \gtrsim 60\%$ (Figure 3c, red and orange curves and stars).

3.3. Deep Continental Roots

[26] At the base of deep continental roots that protrude below the asthenosphere, shear stresses increase more strongly (~5 times), compared to the

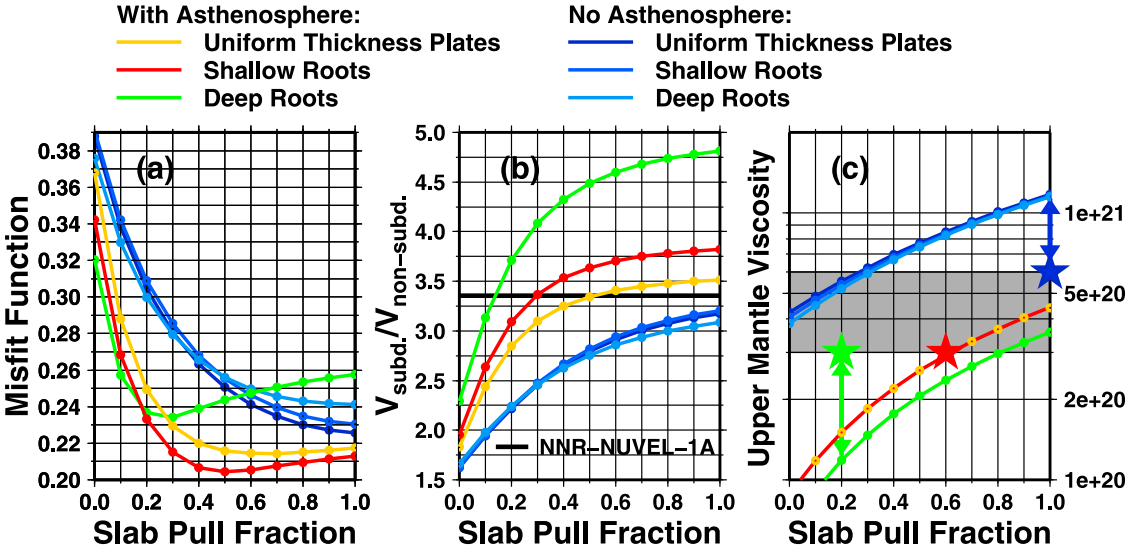

Figure 3. Plate tectonic diagnostics and comparison to observations. (a) Misfit function between calculated and NNR-NUVEL-1A plate motions. (b) Ratio of area-weighted average speed of subducting relative to non-subducting plates ($V_{subd.}/V_{non-subd.}$). (c) Sub-lithospheric upper mantle viscosity required to match the average global plate speed with observations. All diagnostics are plotted as a function of slab pull fraction, f_{sp}. Different models are described in section 2.4. The black line in Figure 3b represents the plate speed ratio for the NNR-NUVEL-1A model [*DeMets et al.*, 1994]. The grey area in Figure 3c represents viscosity estimates for the sub-lithospheric upper mantle of 3–6 $\times$ 10^{20} Pa s, obtained from post-glacial rebound analysis [*Mitrovica*, 1996]. Stars in Figure 3c indicate the viscosities in the post-glacial rebound range that produce global average plate speeds closest to the observations, and that are employed to produce Figure 4.

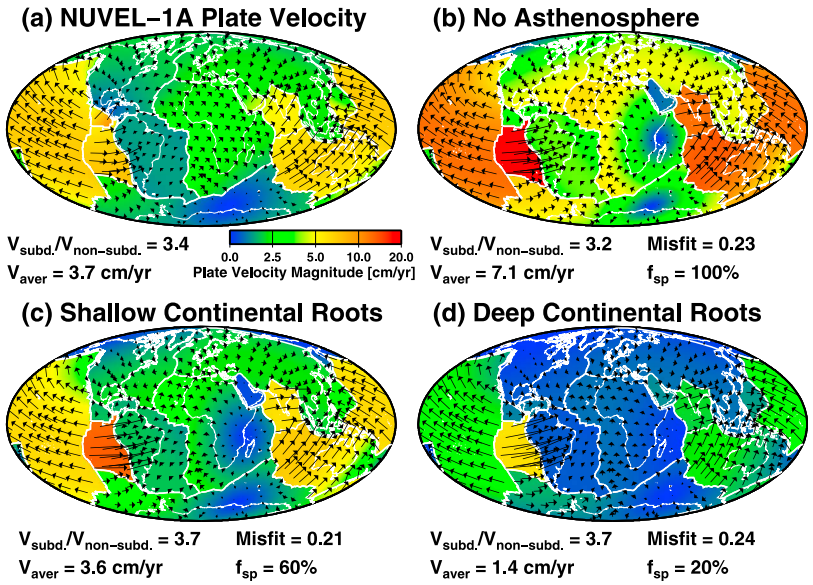

Figure 4. Observed and calculated plate motions. (a) Global pattern of no-net rotation plate motions from model NNR-NUVEL-1A [*DeMets et al.*, 1994]. Calculated plate motions are shown for models with (b) uniform plate thicknesses and no asthenosphere, (c) shallow continental roots with an asthenosphere, and (d) deep continental roots with an asthenosphere. Black arrows represent plate velocity directions in a no-net rotation frame normalized to the global average plate velocity for each case. Colors represent absolute magnitudes of plate motions. Indicated for each case are the assigned slab pull fraction, f_{sp}, the calculated plate speed ratio, $V_{subd.}/V_{non-subd.}$, and the misfit to the NNR-NUVEL-1A plate motions. The global average plate speed, V_{aver}, is calculated for an upper mantle viscosity that falls within the estimated range from post-glacial rebound analysis [*Mitrovica*, 1996] and that is closest to the required viscosity that matches the NNR-NUVEL-1A plate velocity magnitudes, i.e. 6 $\times$ 10^{20} Pa s for Figure 4b and 3 $\times$ 10^{20} Pa s for Figures 4c and 4d (see Figure 3c, arrows and stars).

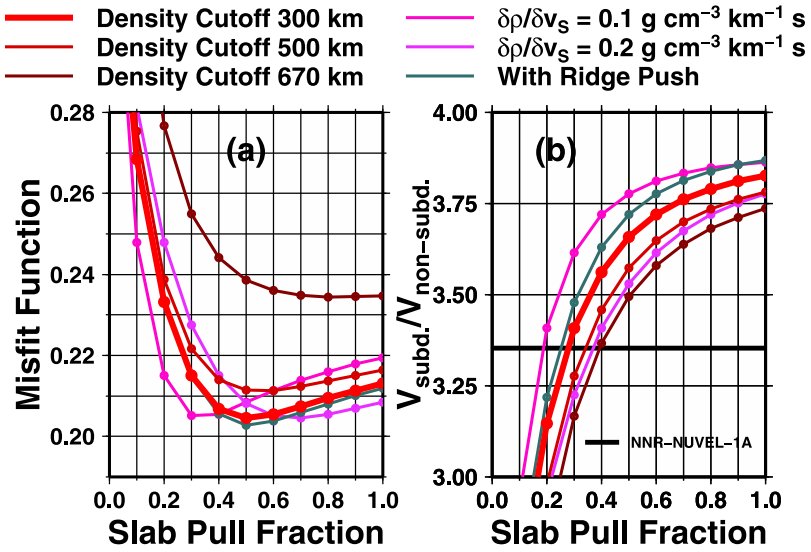

Figure 5. Plate motion diagnostics for models described in section 4. (a) Misfit function between calculated and NNR-NUVEL-1A plate motions. (b) Ratio of area-weighted average speed of subducting relative to non-subducting plates ($V_{subd.}/V_{non-subd.}$). The reference model with shallow roots, tomography conversion factor $\partial\rho/\partial v_S$ = 0.15 g cm^{-3} km^{-1} s, and cutoff depth of mantle density anomalies z_{cut} = 300 km is shown in red, and is the same curve as in Figure 3. Results are shown for 5 models that differ from the reference case by having $\partial\rho/\partial v_S$ = 0.1 g cm^{-3} km^{-1} s (pink curve), $\partial\rho/\partial v_S$ = 0.2 g cm^{-3} km^{-1} s (purple curve), z_{cut} = 500 km (light brown curve), and z_{cut} = 670 km (dark brown curve), and ridge push forces calculated from buoyancy anomalies in the top 100 km of oceanic lithosphere (grey curve).

uniform thickness model (Figures 2g and 2h) because roots mechanically couple to the sub-asthenospheric mantle. With deep roots, overriding plates become notably slower than in either the shallow roots or the uniform thickness case, as reflected by the high plate speed ratio (Figures 3a and 3b, green curves), and the relative impact of slab pull on subducting plates magnifies. However, the presence of anchoring roots by itself (i.e. without slab pull) is insufficient to bring plate motions into agreement with the observations (Figures 3a and 3b, green curves at f_{sp} = 0%). Instead, plate motions fit the observations for a narrow range of small slab pull contributions ($f_{sp} \sim$ 20%, Figures 3a and 3b (green curves) and Figure 4d) and this low value implies globally weak transmission of slab pull forces to surface plates. Figure 4d shows that such weak slab pull contributions result in global average plate speeds (V_{aver} = 1.4 cm yr^{-1}) below the observed value (V_{aver} = 3.7 cm yr^{-1}) for an upper mantle viscosity of 3 × 10^{20} Pa s that corresponds to the lower bound of the post-glacial rebound study by *Mitrovica* [1996] (green star in Figure 3c).

4. Sensitivity Analysis: Influence of Model Parameterization and Ridge Push

[27] To investigate the sensitivity of our results to our model parameterization, we tested the influence of (1) the buoyancy conversion factor $\partial\rho/\partial v_S$, (2) the cutoff depth of mantle density anomalies, z_{cut}, and (3) the forces due to oceanic lithosphere thickening with age (ridge push). We compare test cases to the model with an asthenosphere and shallow continental roots (red curves in Figures 3 and 5 are the same).

[28] We tested velocity-density conversion values in the range $\partial\rho/\partial v_S$ = 0.1 to 0.2 g cm^{-3} km^{-1} s, which reflects current uncertainty in mineral physics data and first principles calculations [e.g., *Karato*, 1993; *Karato and Karki*, 2001; *Stixrude and Lithgow-Bertelloni*, 2007]. Increasing $\partial\rho/\partial v_S$ by a factor of 2, causes mantle buoyancy forces to increase by a factor of 2 and corresponding driving tractions on the lithospheric base increase accordingly. When $\partial\rho/\partial v_S$ and the slab pull fraction f_{sp} are multiplied by the same factor, the misfit and plate speed ratios remain unchanged (Figure 5, cf. pink, red, and purple curves). We verified that a similar trade-off between $\partial\rho/\partial v_S$ and f_{sp} occurs for the other model types.

[29] An increase of z_{cut} from the 300 km reference value to 500 km and 670 km results in a progressively weaker and more diffuse near-surface stress field. This decreased contribution of the upper mantle buoyancy field causes a poorer fit to the observations, as demonstrated by the progressively degrading misfit and decreasing plate speed ratio

(Figure 5, red, light brown, and dark brown curves). This indicates that mantle flow driven by upper mantle structure contributes moderately to driving plate motions, but slab pull edge forces still exert the largest influence.

[30] The force balance of tectonic plates can also be affected by ridge-push forces, although these are likely much less important than slab pull forces [*McKenzie*, 1969; *Richter*, 1975; *Lithgow-Bertelloni and Richards*, 1998]. We approximated the influence of ridge push by including buoyancy in the top 100 km of our model from the same temperature field that is used for computing lithospheric viscosity structure from the thicknesses shown in Figure 1 (in addition to buoyancy below 300 km). Thus, we incorporate buoyancy variations associated with thickening of the oceanic lithosphere as it moves away from spreading ridges. We find that ridge push introduces additional tractions directed away from ridges, as expected, but the net effect on the global force balance is small, as demonstrated by Figure 5 (cf. grey curve to red).

5. Discussion

[31] In our preferred scenario of a globally-extending asthenosphere, continental roots do not protrude below a low-viscosity asthenosphere. We find that the influence of continental roots on calculated plate motions is not significant if a low-viscosity asthenosphere is present below even the deepest roots. Our results are consistent with, and expand upon, 3-D numerical modeling studies that did not include the influence of slab pull edge forces [*Zhong*, 2001; *Becker*, 2006; *Ghosh et al.*, 2010]. Previous geodynamic modeling studies of *Zhong* [2001], *Becker* [2006], and M. Gerault et al. (The role of slabs and oceanic plate geometry for the net rotation of the lithosphere, trench motions, and slab return flow, submitted to *Geochemistry, Geophysics, Geosystems*, 2011) show that strong continental roots cause a sense of lithospheric net rotation that is consistent with hotspot reference frame models. This could suggest the presence of continental roots, independent of other geophysical evidence, although such comparisons are hampered by uncertainty of hotspot motion relative to the stable lower mantle, e.g., due to distortion by global mantle flow [*Steinberger et al.*, 2004]. Our preferred scenario of a globally-extending asthenosphere is consistent with the recent discovery of flow-induced seismic anisotropy beneath continental roots [*Gung et al.*, 2003; *Debayle and Kennett*, 2005; *Yuan and Romanowicz*, 2010] that extend no deeper than ~200–250 km [*Dalton et al.*, 2009]. Coupling of ~50–100% of excess upper mantle slab weights to the surface plates, as suggested by our results, allows for a substantial effect of decoupling mechanisms, for example due to bending resistance [*Chapple and Forsyth*, 1979], slab detachment [*Spakman et al.*, 1988], fault zone resistance, or viscous support of slabs. It is possible that the suggested slab-plate coupling represents a global average of subduction zones with more diverse degrees of coupling. Decoupling mechanisms are difficult to constrain, but local variations could bring the calculated plate motions even closer to the observations.

[32] For our preferred models, predicted plate motions are close to observations for the Pacific, North and South American, Eurasian, Philippine, Australian, and Antarctic plates. Small plates contribute relatively little to the total misfit, but they are also more susceptible to model parameterization (e.g., slab pull, weak zones, lithospheric thickness). This can explain the relatively large deviations from observed motions for the Cocos, Caribbean, and Arabian plates. Two plates that contribute significantly to the residual misfit in our models are the Indian and Nazca plate. India is moving east in our models rather than in the observed north-east direction, which reflects ongoing India-Eurasia continental collision [*Molnar and Tapponnier*, 1975]. This collision is possibly related to ongoing subduction of Indian lithosphere, as suggested by recent regional tomographic data [*Li et al.*, 2008], or plate-driving forces due to active mantle upwelling below the Indian ocean [*Becker and Faccenna*, 2011]. The Nazca plate is moving too fast in the observed eastward direction which suggests that subduction below the Andes may be slowed by slab flattening [*Allmendinger et al.*, 1997] or resisting forces associated with Andean topography [*Husson and Ricard*, 2004; *Meade and Conrad*, 2008].

6. Conclusions

[33] We included lateral variations in rheology in calculations of global plate motions that are dynamically consistent with driving forces associated with subducting slabs and convective mantle flow. Based on our numerical modeling results, we conclude that calculated plate motions can be reconciled with observed plate motions if even the deepest continental roots are underlain by a low viscosity asthenosphere. For such models with a globally extending asthenosphere, an optimum range of $f_{sp} \sim 50$–100% shows that only about half of the excess upper mantle slab weights need to contribute to pull forces.

Continental roots have a negligible influence on calculated plate motions provided that the roots are underlain by a low-viscosity asthenosphere. Calculated patterns of plate motions are also close to observed patterns if continental roots anchor directly to the upper mantle below a low-viscosity asthenospheric layer and slab-plate coupling is relatively weak ($f_{sp} \sim 20\%$), or for models without an asthenosphere and strong slab-plate coupling ($f_{sp} \sim 100\%$). However, both these scenarios are more difficult to reconcile with upper mantle viscosity estimates from post-glacial rebound analysis [*Mitrovica*, 1996]. Our model results that suggest a globally-extending asthenosphere are consistent with recent seismological evidence for flow-induced seismic anisotropy beneath continental roots, and allow for substantial decoupling of slabs of former lithosphere from subducting plates.

Acknowledgments

[34] This work was supported by the U.S. National Science Foundation under grants EAR-0914712 (C.P.C.) and EAR-0609553 (C.L.-B.). We thank Thorsten Becker, Bernhard Steinberger, Wouter Schellart, and an anonymous reviewer for thoughtful comments that helped to improve this paper.

References

Allmendinger, R. W., T. E. Jordan, and S. M. Kay (1997), The evolution of the Altiplano-Puna plateau of the central Andes, *Annu. Rev. Earth Planet. Sci.*, *25*, 139–174.

Alpert, L. A., T. W. Becker, and I. W. Bailey (2010), Global slab deformation and centroid moment tensor constraint on viscosity, *Geochem. Geophys. Geosyst.*, *11*, Q12006, doi:10.1029/2010GC003301.

Alvarez, W. (1982), Geologic evidence for the geographical pattern of mantle return flow and the driving mechanism of plate tectonics, *J. Geophys. Res.*, *87*, 6697–6710.

Becker T. W. (2006), On the effect of temperature and strain-rate dependent viscosity on global mantle flow, net rotation, and plate-driving forces, *Geophys. J. Int.*, *167*, 943–957, doi:10.1111/j.1365-246X.2006.03172.x.

Becker, T. W., and C. Faccenna (2011), Mayor conveyor beneath the Tethyan collisional belt, *Earth Planet. Sci. Lett.*, *310*, 453–461, doi:10.1016/j.epsl.2011.08.021.

Becker, T. W., and R. J. O'Connell (2001), Predicting plate velocities with mantle circulation models, *Geochem. Geophys. Geosyst.*, *2*(12), 1060, doi:10.1029/2001GC000171.

Behn, M. D., C. P. Conrad, and P. G. Silver (2004), Detections of upper mantle flow associated with the African Superplume, *Earth Planet. Sci. Lett.*, *224*, 259–274, doi:10.1016/j.epsl.2004.05.026.

Bilek, S. L., C. P. Conrad, and C. Lithgow-Bertelloni (2005), Slab pull, slab weakening, and their relation to deep intra-slab seismicity, *Geophys. Res. Lett.*, *32*, L14305, doi:10.1029/2005GL022922.

Billen, M. I. (2008), Modeling the dynamics of subducting slabs, *Annu. Rev. Earth. Planet. Sci. 36*, 325–356, doi:10.1146/annurev.earth36.031207.124129.

Buffett, B. A., and A. Heuret (2011), Curvature of subducted lithosphere from Earthquake locations in the Wadati-Benioff zone, *Geochem. Geophys. Geosyst.*, *12*, Q06010, doi:10.1029/2011GC003570.

Burke, K., and J. T. Wilson (1972), Is the African plate stationary?, *Nature*, *239*, 387–390.

Capitanio, F. A., G. Morra, and S. Goes (2007), Dynamic models of downgoing plate-buoyancy driven subduction: Subduction motions and energy dissipation, *Earth Planet. Sci. Lett.*, *262*, 284–297.

Carlson, R. L. (1981), Boundary forces and plate velocities, *Geophys. Res. Lett.*, *8*(9), 958–961, doi:10.1029/GL008i009p00958.

Chapple, W. M., and D. W. Forsyth (1979), Earthquakes and bending of plates at trenches, *J. Geophys. Res.*, *84*, 6729–6749.

Cloos, M. (1993), Lithospheric buoyancy and collisional orogenesis–Subduction of oceanic plateaus, continental margins, island arcs, spreading ridges, and seamounts, *Geol. Soc. Am. Bull.*, *105*(6), 715–737, doi:10.1130/0016-7606.

Conrad, C. P., and M. Gurnis (2003), Seismic tomography, surface uplift, and the breakup of Gondwanaland: Integrating mantle convection backwards in time, *Geochem. Geophys. Geosyst.*, *4*(3), 1031, doi:10.1029/2001GC000299.

Conrad, C. P., and C. Lithgow-Bertelloni (2002), How mantle slabs drive plate tectonics, *Science*, *298*, 207–209, doi:10.1126/science.1074161.

Dalton, C. A., G. Ekström, and A. M. Dziewonski (2009), Global seismological shear velocity and attenuation: A comparison with experimental observations, *Earth Planet. Sci. Lett.*, *284*, 65–75, doi:10.1016/j.epsl.2009.04.009.

Davies, J. H., and F. von Blankenburg (1995), Slab breakoff: A model of lithospheric detachment and its test in the magmatism and deformation of collisional orogens, *Earth Planet. Sci. Lett.*, *129*, 85–102.

Debayle, E., and B. L. N. Kennett (2005), Global azimuthal seismic anisotropy and the unique plate-motion deformation of Australia, *Nature*, *433*(7025), 509–512, doi:10.1038/nature03247.

DeMets, C., R. G. Gordon, D. F. Argus, and S. Stein (1990), Current plate motions, *Geophys. J. Int.*, *101*, 425–478.

DeMets, C., R. G. Gordon, D. F. Argus, and S. Stein (1994), Effect of recent revisions to the geomagnetic reversal time scale on estimates of current plate motions, *Geophys. J. Int.*, *21*(20), 2191–2194.

Elsasser, W. M. (1969), Convection and stress propagation in the upper mantle, in *The Application of Modern Physics to the Earth and Planetary Interiors*, edited by S. K. Runkorn, pp. 223–246, Wiley-Interscience, London.

Forsyth, D., and S. Uyeda (1975), On the relative importance of the driving forces of plate motion, *Geophys. J. R. Astron. Soc.*, *43*, 163–200.

Forte, A. M., R. Moucha, R. D. B. Rowley, S. Quéré, J. X. Mitrovica, N. A. Simmons, and S. P. Grand (2009), Recent tectonic plate decelerations driven by mantle convection, *Geophys. Res. Lett.*, *36*, L23301, doi:10.1029/2009GL040224.

Gerya, T. V., D. A. Yuen, and M. V. Maresch (2004), Thermomechanical modelling of slab detachment, *Earth Planet. Sci. Lett.*, *226*, 101–116, doi:10.1016/j.epsl.2004.07.022.

Ghosh, A., T. W. Becker, and S. J. Zhong (2010), Effect of lateral viscosity variations on the geoid, *Geophys. Res. Lett.*, *37*, L01301, doi:10.1029/2009GL040426.

Gripp, A. E., and R. G. Gordon (2002), Young tracks of hotspots and current plate velocities, *Geophys. J. Int.*, *150*(2), 321–361, doi:10.1046/j.1365-246X.2002.01627.x.

Gung, Y., M. Panning, and B. Romanowicz (2003), Global anisotropy and the thickness of continents, *Nature*, *422*, 707–711, doi:10.1038/nature01559.

Hager, B. H. (1984), Subducted slabs and the geoid: Constraints on mantle rheology and flow, *J. Geophys. Res.*, *89*(B7), 6003–6015.

Hirth, G., R. L. Evans, and A. D. Chave (2000), Comparison of continental and oceanic mantle electrical conductivity: Is the Archean lithosphere dry?, *Geochem. Geophys. Geosyst.*, *1*(12), 1030, doi:10.1029/2000GC000048.

Husson, L., and Y. Ricard (2004), Stress balance above subduction: Application to the Andes, *Earth Planet. Sci. Lett.*, *222*, 1037–1050, doi:10.1016/j.epsl.2004.03.041.

Isacks, B., and P. Molnar (1971), Distribution of stresses in the descending lithosphere from a global survey of focal-mechanism solutions of mantle earthquakes, *Rev. Geophys.*, *9*(1), 103–175.

Jordan, T. H. (1975), The continental tectosphere, *Rev. Geophys.*, *13*(3), 1–12, doi:10.1029/RG013i003p00001.

Karato, S. (1993), Importance or anelasticity in the interpretation of seismic tomography, *Geophys. Res. Lett.*, *20*(15), 1623–1626, doi:10.1029/93GL01767.

Karato, S.-I., and B. B. Karki (2001), Origin of lateral variation of seismic wave velocities and density in the deep mantle, *J. Geophys. Res.*, *106*(B10), 21,771–21,783, doi:10.1029/2001JB000214.

Kaufmann, G., and K. Lambeck (2000), Mantle dynamics, postglacial rebound and the radial viscosity profile, *Phys. Earth Planet. Int.*, *121*(3–4), 301–324, doi:10.1016/S0031-9201(00)00174-6.

Kellogg, L. H., B. H. Hager, and R. D. van der Hilst (1999), Compositional stratification in the deep mantle, *Science*, *283*, 1881–1884.

Lallemand, S., A. Heuret, and D. Boutelier (2005), On the relationships between slab dip, back arc stress, upper plate absolute motion, and crustal nature in subduction zones, *Geochem. Geophys. Geosyst.*, *6*, Q09006, doi:10.1029/2005GC000917.

Lambeck, K., and P. Johnston (1998), The viscosity of the mantle: Evidence from analyses of glacial-rebound phenomena, in *The Earth's Mantle*, edited by I. Jackson, pp. 461–502, Cambridge Univ. Press, Cambridge, U. K.

Le Pichon, X. (1968), Sea-floor spreading and continental drift, *J. Geohys. Res.*, *73*(12), 3661–3697.

Li, C., R. D. van der Hilst, A. S. Meltzer, and E. R. Engdahl (2008), Subduction of the Indian lithosphere beneath the Tibetan Plateau and Burma, *Earth Planet. Sci. Lett.*, *274*, 157–168, doi:10.1016/j.epsl.2008.07.016.

Lithgow-Bertelloni, C., and M. A. Richards (1998), The dynamics of Cenozoic and Mesozoic plate motions, *Rev. Geophys.*, *36*, 27–78.

McKenzie, D. (1969), Speculations on the consequences and causes of plate motions, *Geophys. J. R. Astron. Soc.*, *18*, 1–32.

Meade, B. J., and C. P. Conrad (2008), Andean growth and the deceleration of South American subduction: Time evolution of a coupled orogen-subduction system, *Earth Planet. Sci. Lett.*, *275*, 93–101.

Minster, J. B., T. H. Jordan, P. Molnar, and E. Haines (1974), Numerical modelling of instantaneous plate tectonics, *Geophys. J. R. Astron. Soc.*, *36*, 541–576.

Mitrovica J. X. (1996), Haskell [1935] revisited, *J. Geophys. Res.*, *101*(B1), 555–569, doi:10.1029/95JB03208.

Molnar, P., and P. Tapponnier (1975), Cenozoic tectonics of Asia: Effects of a continental collision, *Science*, *189*(4201), 419–421, doi:10.1126/science.189.4201.419.

Morgan, W. J. (1971), Convecting plumes in the lower mantle, *Nature*, *230*, 42–43.

Müller, R. D., W. R. Roest, J.-W. Royer, L. M. Gahagan, and J. G. Sclater (1997), Digital isochrons of the world's ocean floor, *J. Geophys. Res.*, *102*, 3211–3214, doi:10.1029/96JB01781.

Parmentier, E. M., D. L. Turcotte, and K. E. Torrance (1976), Studies of finite amplitude non-Newtonian thermal convection with application to convection in the Earth's mantle, *J. Geophys. Res.*, *81*(11), 1839–1846, doi:10.1029/JB081i011p01839.

Ricard, Y., and C. Vigny (1989), Mantle dynamics with induced plate-tectonics, *J. Geophys. Res.*, *94*(B12), 17,543–17,559, doi:10.1029/JB094iB12p17543

Ricard, Y., C. Vigny, and C. Froidevaux (1989), Mantle heterogeneities, geoid, and plate motion: A Monte Carlo inversion, *J. Geophys. Res.*, *94*(B10), 13,739–13,754, doi:10.1029/JB094iB10p13739.

Ricard, Y., M. Richards, C. Lithgow-Bertelloni, and Y. Le Stunff (1993), A geodynamic model of mantle density heterogeneity, *J. Geophys. Res.*, *98*(B12), 21,895–21,909, doi:10.1029/93JB02216.

Richter, F. M. (1975), On the driving mechanisms of plate tectonics, *Tectonophysics*, *38*(1–2), 61–88, doi:10.1016/0040-1951(77)90201-3.

Ritsema, J., H. J. van Heijst, and J. H. Woodhouse (2004), Global transition zone tomography, *J. Geophys. Res.*, *109*, B02302, doi:10.1029/2003JB002610.

Rudnick, R., W. McDonough, and R. O'Connell (1998), Thermal structure, thickness and composition of continental lithosphere, *Chem. Geol.*, *145*, 395–411.

Schellart, W. P. (2004), Quantifying the net slab pull force as a driving mechanism for plate tectonics, *Geophys. Res. Lett. 31*, L07611, doi:10.1029/2004GL019528.

Solomon, S. C., and N. H. Sleep (1974), Some simple physical models for absolute plate motions, *J. Geophys. Res.*, *79*, 2557–2567.

Spakman, W., M. J. R. Wortel, and N. J. Vlaar (1988), The Hellenic subduction zone: a tomographic image and its geodynamic implications, *Geophys. Res. Lett.*, *15*(1), 60–63.

Stadler, G., M. Gurnis, C. Burstedde, L. C. Wilcox, L. Alisic, and O. Ghattas (2010), The dynamics of plate tectonics and mantle flow: From local to global scales, *Science*, *329*, 1033–1038, doi:10.1126/science.1191223.

Steinberger, B., R. Sutherland, and R. J. O'Connell (2004), Prediction of Emperor-Hawaii seamount locations from a revised model of global plate motion and mantle flow, *Nature*, *430*(6996), 167–173, doi:10.1038/nature02660.

Steiner, S. A., and C. P. Conrad (2007), Does active upwelling help drive plate motions?, *Phys. Earth Planet. Sci.*, *161*, 103–114, doi:10.1016/j.pepi.2007.01.005.

Stixrude, L., and C. Lithgow-Bertelloni (2007), Influence of phase transformations on lateral heterogeneity and dynamics in Earth's mantle, *Earth Planet. Sci. Lett.*, *263*, 45–55.

Tao, W. C., and R. J. O'Connell (1993), Deformation of a weak subducted slab and variation of seismicity with depth, *Nature*, *361*, 626–628.

van der Hilst, R. D., E. R. Engdahl, W. Spakman, and G. Nolet (1991), Tomographic imaging of subducted lithosphere below Pacific island arcs, *Nature*, *353*, 37–43, doi:10.1038/353037a0.

van Dinther, Y., G. Morra, F. Funiciello, and C. Faccenna (2010), Role of the ovverriding plate in the subduction

process: Insights from numerical models, *Tectonophysics*, *484*, 74–86, doi:10.1016/j.tecto.2009.08.038.

van Summeren, J. (2008), Constraints on thermo-chemical convection from numerical modelling and geophysical data, PhD thesis, Utrecht Univ., Utrecht, Netherlands.

van Thienen, P., J. van Summeren, R. D. van der Hilst, A. P. van den Berg, and N. J. Vlaar (2005), Numerical study of the origin and stability of chemically distinct reservoirs deep in Earth's mantle, in *Earth's Deep Mantle: Structure, Composition, and Evolution*, *Geophys. Monogr. Ser.*, vol. 160, edited by R. D. van der Hilst et al., pp. 117–136, AGU, Washington, D. C., doi:10.1029/160GM09.

Wu, B., C. P. Conrad, A. Heuret, C. Lithgow-Bertelloni, and S. Lallemand (2008), Reconciling strong slab pull and weak plate bending: The plate motion constraint on the strength of mantle slabs, *Earth Planet. Sci. Lett.*, *272*, 412–421, doi:10.1016/j.epsl.2008.05.009.

Yuan, H., and B. Romanowicz (2010), Lithospheric layering in the North American craton, *Nature*, *466*, 1063–1068, doi:10.1038/nature09332.

Zhong, S. (2001), Role of ocean-continent contrast and continental keels on plate motions, net rotation of the lithosphere, and the geoid, *J. Geophys. Res.*, *106*, 703–712, doi:10.1029/2000JB900364.

Zhong, S., M. T. Zuber, L. N. Moresi, and M. Gurnis (2000), The role of temperature-dependent viscosity and surface plates in spherical shell models of mantle convection, *J. Geophys. Res.*, *105*, 11,063–11,082, doi:10.1029/2000JB900003.